Quantification and Characterization of Regional Seismic Signals from Cast Blasting in Mines: *A Linear Elastic Model*

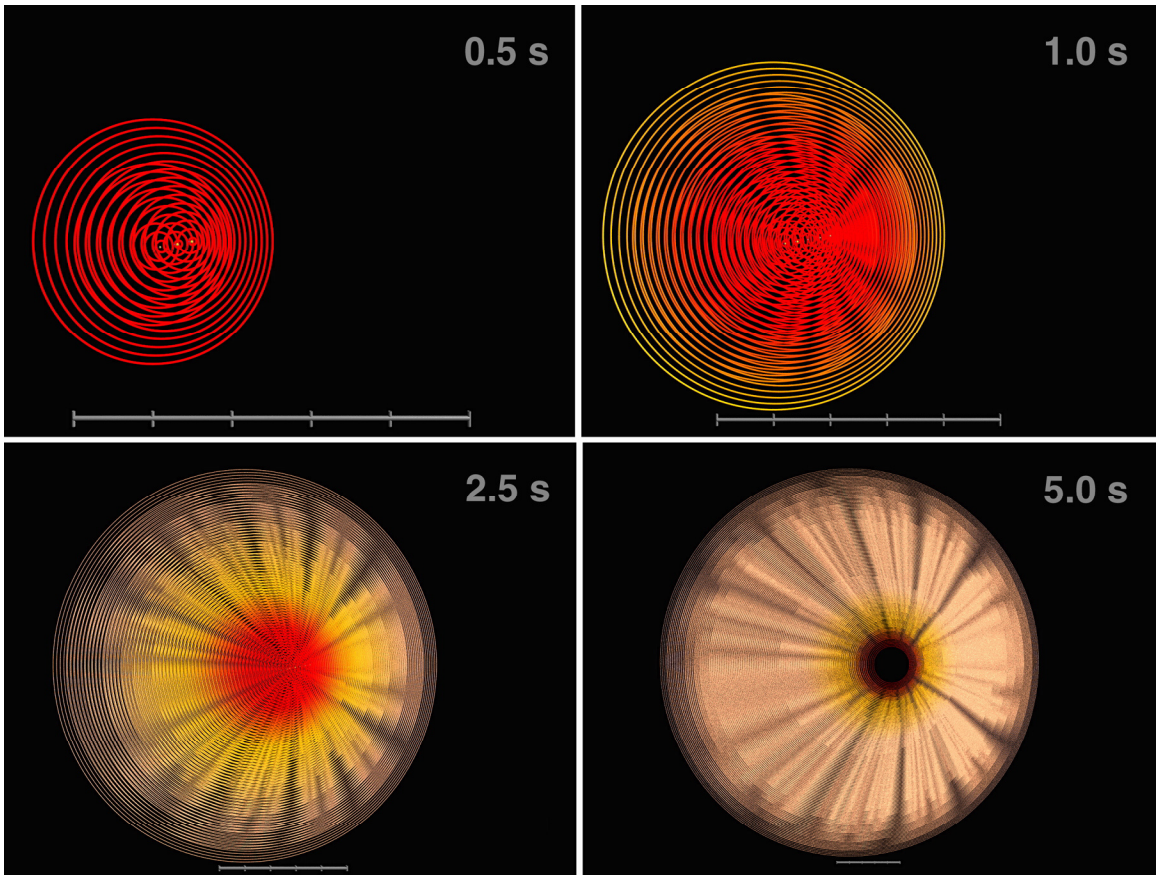

Sridhar Anandakrishnan*
Steven R. Taylor
Brian W. Stump
Earth and Environmental Sciences Division
Los Alamos National Laboratory
University of California
Los Alamos, NM 87545

*Now at
Pennsylvania State University
Earth Systems Science Center
248 Deike
University Park, PA 16802

November 12, 1996
LAUR-96-3747
Submitted to *Geophys . J. Int.*

Abstract

Cast blasts in coal mines, designed to move large volumes of overburden, are a source of large (1-5 kt), frequent explosions in parts of the world with near-surface coal resources. Mining events of this source type are triggering the prototype International Monitoring System for the Comprehensive Test Ban Treaty being tested under the Group of Scientific Experts Technical Test 3 (GSETT-3). We wish to develop techniques to distinguish between the seismic signals produced by these explosions and equivalent size single (or point) sources. To that end, we have developed a linear elastic model to simulate regional-distance seismograms from mining cast blasts. Cast blasting involves a shot-array with delayed detonations casting rock horizontally into a pit. We model the effects of the milli-second delay firing pattern, the depth of the pit, and the cast of material into the pit. We attempt to separate the effects due to the explosion, the vertical movement of mass, and the horizontal movement of mass in order to produce a physical understanding of the resulting waveforms which can be used to assess potential discriminants for these types of explosions. These physical models of source processes are constrained by numerous near-surface measurements of cast blasts in NE Wyoming that are triggering GSETT-3. Two observational results at regional distances that are replicated by these models are the excitation of 10-20 sec surface waves by the cast blasts and the insensitivity of peak amplitude to total explosive size for normal blasting practices. The insensitivity of peak amplitudes from the cast blast to total source size is a consequence of the delay firing practice under normal procedures. This practice was initiated to reduce ground motions in the near-source region around the mine and it appears that it is also successful in controlling peak amplitudes at regional distances. In our model of cast blasting we have included the effects due to mass transfer into an excavated pit after the blast. This mass transfer has both a vertical and horizontal force component, each of which contribute to the final seismogram, the latter azimuthally dependent. Assuming maximum coupling, the contribution to the seismogram due to the vertical force component is approximately equal to the explosion contribution for pit depths of zero to 10 m, but dominates for pit depths of 20 m or greater. The contribution due to the horizontal force component is mainly in the enhanced R_g. Comparison of high-frequency seismic radiation from the single shot and cast blast shows little qualitative difference in the regional waveforms.

Introduction

Monitoring a Comprehensive Test Ban Treaty (CTBT) will require the detection, location and identification of a number of source types including earthquakes, mine explosions, mine collapses and rock bursts. The seismic signals generated by each will be used to assess whether the event has any characteristics like a single fired nuclear explosion. Analysis of preliminary results from the GSETT-3 experiment demonstrates that mining explosions are triggering the prototype International Monitoring System and thus will have to be included in this event identification process (Stump *et al.,* 1996). One type of mine explosion that uses a large amount of explosives (1-5 kiloton (kt)) and is triggering GSETT-3 are coal overburden cast blasts. In a number of geological conditions worldwide, economic coal deposits are found relatively close (<100 m) to the surface. One method of coal recovery utilized under these situations is to construct a pit that extends to the bottom of the coal and then explosively move the overburden above the coal into the adjacent pit thus exposing the coal for recovery. In practice, the explosives are used to remove a portion of the overburden and fracture the remainder which is dug with a dragline (a large bucket with volume of ~100 m^3 pulled by steel cables used to remove overburden). Overburdens of one to two hundred feet can require individual explosive boreholes with 5,000 to 10,000 lb. Cast blasts can include as many as 1,000 individual boreholes delay fired over several seconds in order to maximize mass movement while minimizing high frequency peak amplitudes. The explosive array consists of rows of holes parallel to the free face of the mine, and the aim of the time delay between rows is to ensure that the front rows (closest to the face) fractures the rock and begins to move material into the pit before a similar process is initiated in subsequent rows. Practically, cast blasts can include as many as 9 rows. The casting process is quite effective in the first several rows of the shot but the back rows are primarily fractured thus reducing shear

strength and allowing flow into the space exposed by the first few rows. Typically 20-30% of the overburden is cast into its final position and does not require further movement to expose the coal. A dragline is used to remove the remainder of the fractured overburden and expose the coal for recovery. The length of the working face is on the order of 1 to 5 km; the highwall (free face) of the Black Thunder Coal Mine (BT) south pit is 4 km long (Stump *et al.*, 1996).

One possible scenario for evasion of a Comprehensive Test Ban Treaty is to attempt to mask a small nuclear test (< 2 kt) in cast blast explosions routinely conducted as part of coal extraction operations. Previous investigators have studied the spectral "scalloping" from milli-second delay explosions and attempted to use that as a basis for discrimination (Harris and Clark, 1990, Hedlin *et al.*, 1990; Smith, 1989; Smith, 1993). The large number of individual explosions employed during cast blasting, in combination with the design goal of casting material, produces complex time series that are unlike the more impulsive explosions designed only to fracture material (coal shots). In addition to these temporal effects, the model used to represent the source array is extended by adding a horizontal spall component as well as a vertical spall and mass transfer component (e.g. McLaughlin *et al.*, 1993) accounting for the casting process.

The total explosive energy (and possibly the seismic energy) of the cast blast is comparable to a possible decoupled nuclear explosion (that could be detonated simultaneously). On the basis of modeling and observations, Smith (1993) concluded that a simultaneous explosion of greater than 5 to 15% of the total explosive-source array yield would dominate the seismic record. The cast blast can generate a complex waveform due to the mass movement and the millisecond delay-firing. This complexity may complicate discrimination efforts (Hedlin *et al.*, 1989) and it is important to understand the relative contributions of the different elements of these seismic sources. In this paper, we discuss the model and produce synthetic seismograms to parameterize the source. Qualitative

comparisons are made to data collected from sources at the Black Thunder Mine recorded at the regional array, PDAR, near Pinedale, Wyoming.

We have now conducted experiments in the Powder River Basin that include the recording of a modest single fired explosion (40,000-50,000 lb.), cast blasts (3,000,000 to 8,000,000 lb.) and coal shots (3,000 - 500,000 lb.; Stump *et al*., 1996). All these sources have generated regional seismic signals that, in conjunction with near-source phenomenology, will provide the constraints necessary to refine the models developed in this paper. Once these simple models are refined to the extent that they can explain the general character of the regional signals, they can then be used as a guide to assess the effects of other blasting practices and scenarios. Although these studies are focused on large scale cast blasting because of the large amount of explosives used in these processes and the fact that these sources are triggering the prototype International Monitoring System, the same tools can then be applied to other types of blasting such as that associated with the recovery of minerals from hard rock where the primary purpose of the explosions is to fracture the material.

The cast blasts are quite long in duration which may provide a unique characteristic that can be exploited in our analysis of the regional seismograms. Preliminary local magnitudes (M_L) for cast blasts from NE Wyoming reported by GSETT-3 suggest that they are between 3.5 and 4.3. The duration of the accompanying explosions can be in excess of 4 seconds, much longer than a comparable earthquake or a nuclear explosion. Observation of the excitation of 10 to 20 second surface waves suggests that the source duration is observable. The modeling technique described in this paper provides the opportunity to understand these effects and determine robustness of discriminants based upon such observations.

A second important outcome of the empirical work in quantifying these sources is the frequency of abnormal blasting practices. For example, twice in the last year during large

cast blasts (>4,000,000 lb.) we have documented the simultaneous (and probably sympathetic) detonation of a number of boreholes near the end of a blast (Stump *et al.*, 1996). In one case, we estimated that as much as 500,000 lb. of explosives were simultaneously detonated. The models developed in this study provide a mechanism for determining the effect of such simultaneous detonations on the regional (and near-source) waveforms. Experts from the blasting community have estimated that as many as 1 in 20 (or more) explosions detonate abnormally (Chiappetta, personal communication, 1996). The modeling simulations will allow us to understand these sources and possibly reduce false alarms under a CTBT.

Cast-Blast Source Model

To quantify the parameters involved in characterizing a cast blast, a simple model was formulated to represent the following components of the source:

1. The individual explosion of each hole.
2. The horizontal fracture ($z = h$) and vertical spalling of the mass.
3. The vertical fracture ($x\cos\phi + y\sin\phi = 0$) and horizontal spalling of mass in the direction relative to x (where ϕ is the azimuth of the casting direction).
4. The converted energy due to the vertical transport of mass falling into the pit with free face height h_{ff}.
5. The effect of superposition of hundreds of these events in the array with varying time delays.

The model is similar in many ways to the quarry blast model described by McLaughlin *et al.*, (1993). The equivalent moment tensor formulation for this model was then convolved with the regional Green's functions to produce the synthetic waveforms. In anticipation of future work with data from BT and PDAR (Pinedale Seismic Array, Pinedale, Wyoming; Figure 1), we used an earth velocity model for eastern Wyoming (simplified from Prodehl (1979); Figure 2) and calculated the Green's functions for a source at BT and a receiver at PDAR. To calculate the synthetic Green's functions we used the technique of Kennett (1983). The salient parameters are: Nyquist frequency of 10 Hz,

maximum slowness of 0.4 $s \cdot km^{-1}$, range of 360 km, azimuth of 240 degrees, and frequency-independent attenuation in the upper kilometer of the crust.

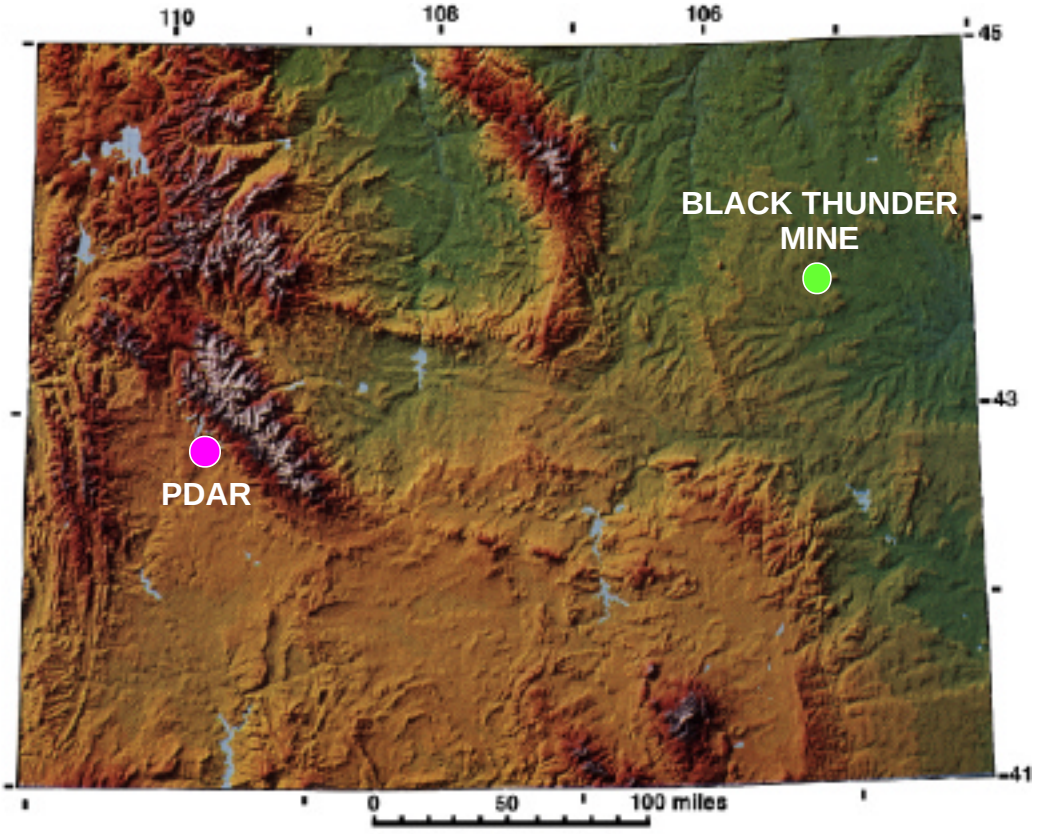

Figure 1. Topographic and location map of Wyoming showing the Black Thunder Mine (BT) and the Pinedale seismic array location (PDAR).

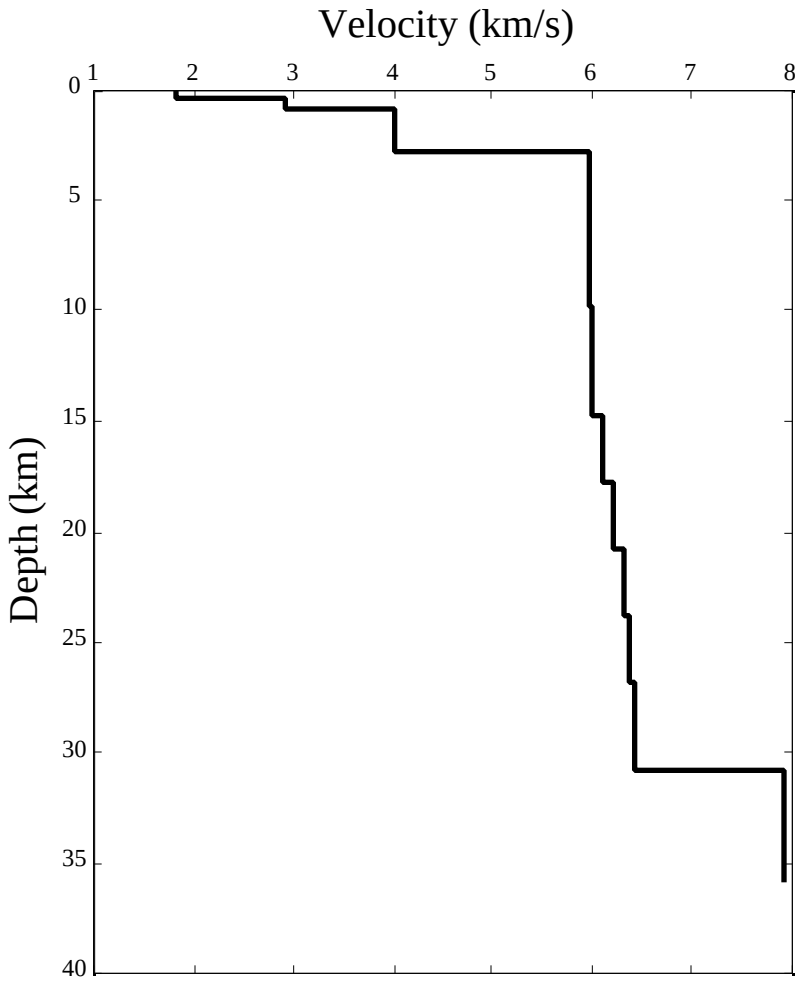

Figure 2. P-velocity model used in waveform synthesis for path between Black Thunder Mine and PDAR.

In Figure 3, the relevant Green's function components for the vertical motions, $G_{zz,z}$, $G_{zx,x}$, $G_{zy,y}$, and $G_{zx,y}$ are shown. The scale is [m·s^{-1} /10^{15} N·m] (i.e., scaled to 10^{15} N·m). The full set of Green's functions associated with the moment tenors representation of the source, $G_{ni,j}$, are not needed for explosions and spall and so we retain only the components $\mathbf{G}$=[$G_{nx,x}$, $G_{nx,y}$, $G_{ny,y}$, $G_{nz,z}$]'.

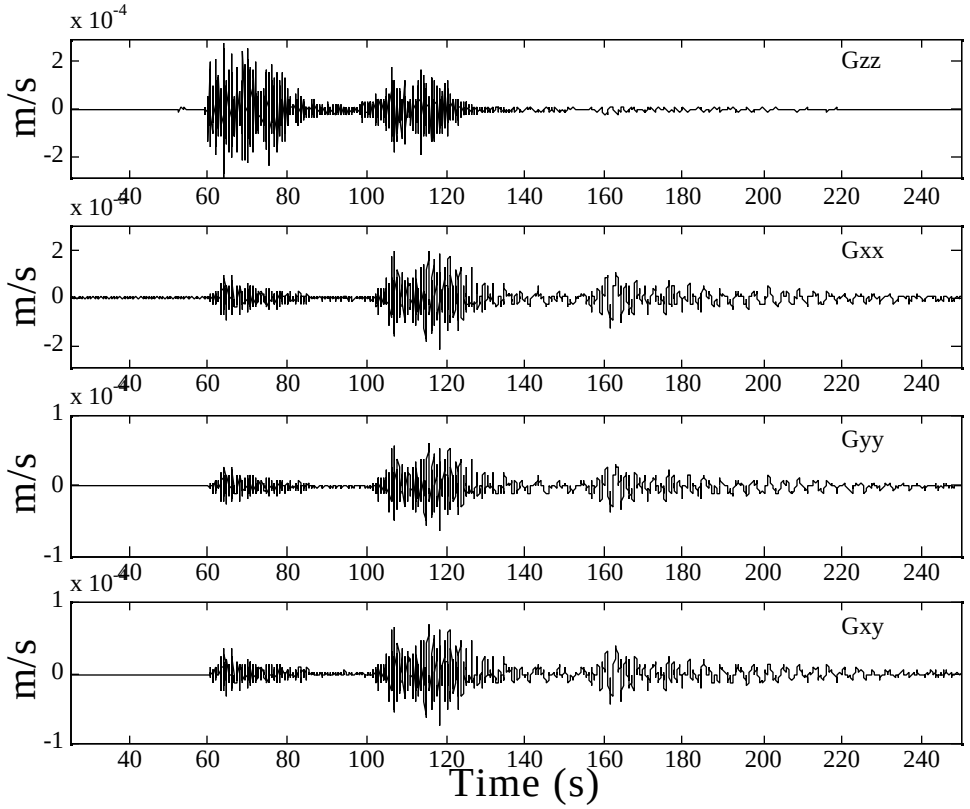

Figure 3. Synthetic Green's functions $G_{zz,z}$, $G_{zx,x}$, $G_{zy,y}$, and $G_{zx,y}$ for a 10^{15} N*m step-function source at BT and receiver at PDAR with velocity model from Figure 2. P_n occurs at about 53 s, P_g at 60 s, L_g at 100 s, and R_g at 160 s.

Next we produced the seismograms related to each component of the source outlined above: the explosion, the vertical component of spall (opening horizontal crack, unloading of the earth, and slapdown with possibly an extra force due to the mass transfer into the pit), and the horizontal spall (the opening vertical crack and the horizontal component of the slapdown). These are shown graphically as point force equivalents in Figure 4.

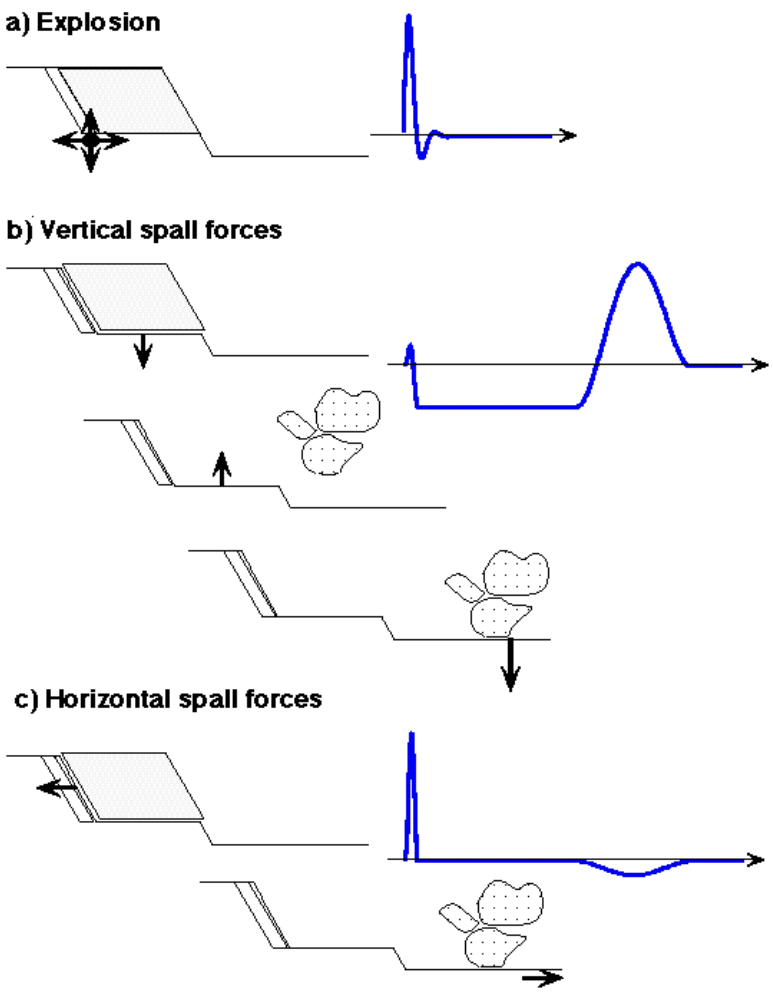

Figure 4. Graphical illustration of the point forces resulting from a cast blast into a pit. The vertical forces are the opening crack and the unloading of the earth followed by impact. The horizontal forces are the opening crack and the horizontal component of the impact.

To illustrate the contributions of the mass transfer into the pit, we separate out the vertical forces $f_v(t)$ into $f_v(t) = f_{v1}(t) + f_{v2}(t)$. Here, f_{v1} is the opening horizontal crack, the subsequent unloading, and the component of the slapdown that would have been present even without the mass transfer into the pit (Figure 4b and Equation 1, below). The force due to the mass-transfer into the pit is represented as f_{v2} (Equation 2) and the horizontal force is $f_h(t)$ (Equation 3; horizontal spall initiation and horizontal component of

the subsequent impact). We modify the source force time functions of Stump (1985, Equation 5):

$$
\begin{aligned}
f_{v1}(t) = {} & \left[m_T \left(\frac{30t^4}{T_{sr}^5} - \frac{60t^3}{T_{sr}^4} + \frac{30t^2}{T_{sr}^3} \right) V_0 \left(H(t) - H(t - T_{sr}) \right) \right] - \\
& m_T g \left[\left\{ \left(\frac{6t^5}{T_{sr}^5} - \frac{15t^4}{T_{sr}^4} + \frac{10t^3}{T_{sr}^3} \right) \left(H(t) - H(t - T_{sr}) \right) \right\} + \right. \\
& \left(H(t - T_{sr}) - H(t - T_S) \right) + \\
& \left\{ \left[1 - \left(\frac{6(t - T_S)^5}{T_{sr}^5} - \frac{15(t - T_S)^4}{T_{sr}^4} + \frac{10(t - T_S)^3}{T_{sr}^3} \right) \right] \times \right. \\
& \left. \left. \left(H(t - T_S) - H(t - T_{sf}) \right) \right\} \right] + \\
& \left[m_T \left(\frac{30(t - T_S)^4}{T_{sr}^5} - \frac{60(t - T_S)^3}{T_{sr}^4} + \frac{30(t - T_S)^2}{T_{sr}^3} \right) V_0 \times \right. \\
& \left. \left(H(t - T_S) - H(t - T_S - T_{sf}) \right) \right]
\end{aligned}
\tag{1}
$$

$$
\begin{aligned}
f_{v2}(t) = {} & \left[m_T \left(\frac{30(t - T_S)^4}{T_{sr}^5} - \frac{60(t - T_S)^3}{T_{sr}^4} + \frac{30(t - T_S)^2}{T_{sr}^3} \right) V_1 \times \right. \\
& \left. \left(H(t - T_S) - H(t - T_S - T_{sf}) \right) \right]
\end{aligned}
\tag{2}
$$

$$
\begin{aligned}
f_h(t) = {} & \left[m_T \left(\frac{30t^4}{T_{sr}^5} - \frac{60t^3}{T_{sr}^4} + \frac{30t^2}{T_{sr}^3} \right) V_h \left(H(t) - H(t - T_{sr}) \right) \right] - \\
& \left[m_T \left(\frac{30(t - T_S)^4}{T_{sf}^5} - \frac{60(t - T_S)^3}{T_{sf}^4} + \frac{30(t - T_S)^2}{T_{sf}^3} \right) V_h \times \right. \\
& \left. \left(H(t - T_S) - H(t - T_S - T_{sf}) \right) \right]
\end{aligned}
\tag{3}
$$

where V_o and V_1 are the initial vertical spall velocity and the impact vertical velocity, respectively, and V_h is the horizontal velocity for both spall and impact. We have modified the time function to allow for two pulse widths: the initial crack opening pulse width T_{sr} and the final impact pulse width T_{sf}. For a vertical spall with no free face, we assume $T_{sr} = T_{sf}$, but examination of video images of a casting shot at BT shows that $T_{sf} \approx 2$ s

(Stump *et al.,* 1996). The spall mass m_T is estimated using the Sobel (1978) scaling of 9.6×10^9 kg per kt of yield.

The estimate of the spalled mass is one of the largest sources of uncertainty in our modeling. Relationships between explosion yield and spalled mass have been published for underground nuclear explosions (e.g. Viecelli, 1973; Sobel, 1978; Patton, 1990) and may not be applicable to mining explosions. Existing models vary by over an order of magnitude in their prediction of total spalled mass. For example, the Sobel mass estimate is about a factor of 6 larger than that of Viecelli which can be enough to bracket the predicted seismic amplitudes from an accompanying explosion (Taylor and Randall, 1989). Additional uncertainties arise due to questions about how the mass movement actually couples into the earth. For example, there can be as much as 30% bulking for the material cast into the pit with the possible collapse of air voids providing a loss mechanism at impact that will reduce the resulting seismic signal.

We *a priori* set the vertical spall velocity V_0 and then determine the horizontal velocity by $V_h = V_0 / \tan\theta$, where θ is the mass-ejection angle (relative to the horizontal). The vertical spall velocity $V_0 = 0.5$ m·s^{-1} is based on examination of near-source accelerograms. The mass ejection angle can be estimated from digitized video images of the blasts. The spall dwell time T_s is

$$T_S = \frac{2V_0}{g} + \sqrt{\frac{2h_{ff}}{g}} \qquad (4)$$

where h_{ff} is the vertical distance the center of mass of the cast material travels before impacting the floor of the pit and g is the gravitational acceleration. The force time functions are shown in Figure 5.

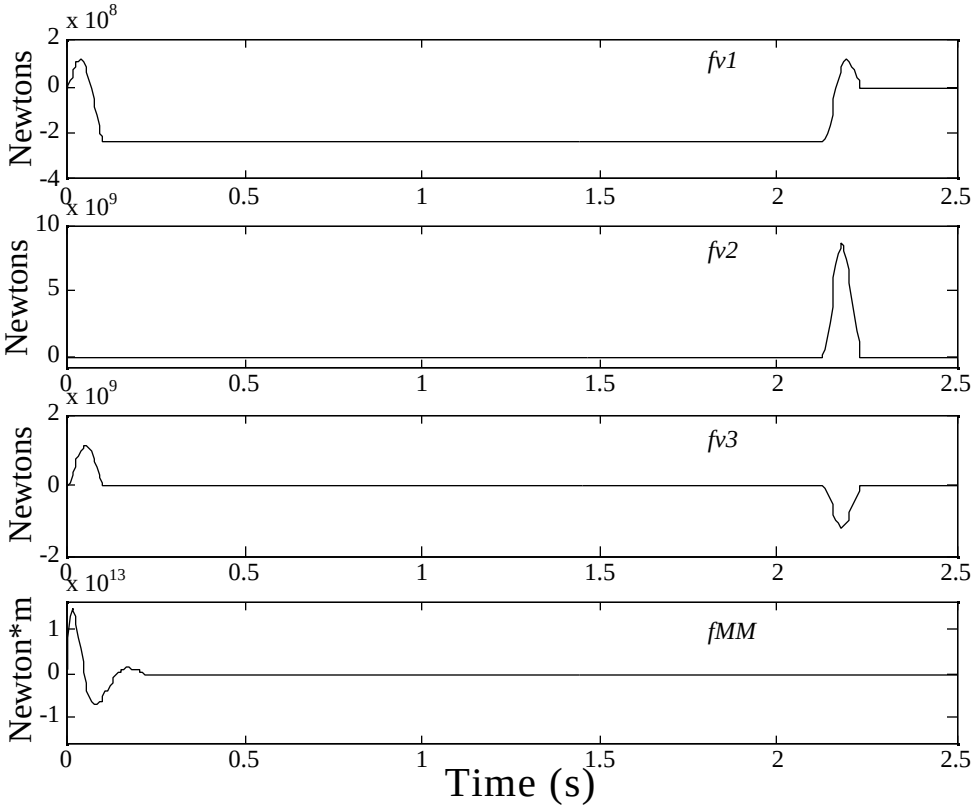

Figure 5. Graphical illustration of the point forces resulting from a cast blast into a pit. The vertical forces are the opening crack and the unloading of the earth followed by impact (vertical spall, f_{v1}) and mass transfer into the pit (f_{v2}). The horizontal forces are the opening crack and the horizontal component of the impact (f_{v3}). The explosion time function is computed using a Mueller-Murphy source model. See text for details.

We then represent the source time function for a pure explosion with a Mueller-Murphy source function f_{MM} (Mueller and Murphy, 1975; Stump, 1985; Figure 5) for an explosion of 0.0025 kt (5,000 lbs), detonated at a depth of 40 m in wet tuff (v_p = 1900 m/s, v_s = 900 m/s, ρ = 1800 kg/m^3). The moment tensor for an explosion is simply the identity matrix I scaled by f_{MM}. Although these are cylindrical explosive boreholes, we follow the work of Reamer *et al.* (1992b) and use the Mueller-Murphy source time function to represent the explosion part of the source representation. The coupling efficiency of the individual explosions, as well as the contribution of the cast material, will require further exploration as the source models are refined.

To calculate the synthetics we use the seismic moment density tensor *m* (Aki and Richards, 1980, Equation. 3.20):

$$m_{pq} = \lambda \nu_k \left[u_k(\xi,\tau)\right]\delta_{pq} + \mu(\nu_p\left[u_q(\xi,\tau)\right] + \nu_q\left[u_p(\xi,\tau)\right] \qquad (5)$$

where [**u**] is the displacement discontinuity across the fault surface, ν is the normal to the fault, ξ is the location of the fault, and τ is time. For a horizontal tension crack with purely vertical displacement (**u** = [0, 0, [u_3]] and ν = [0,0,1]), the diagonal elements of *m* are $\mathrm{diag}(m) = \left[\lambda,\lambda,(\lambda+2\mu)\right]\left[u_3(\xi,\tau)\right]$. For a vertical tension crack, $\mathbf{u} = \left[|u|\sin\phi,|u|\cos\phi,0\right], \nu = \left[\sin\phi,\cos\phi,0\right]$ where $|u|$ is the horizontal displacement, λ and μ are the Lame constants, and ϕ is the azimuth of the crack normal (measured clockwise from north). The diagonal elements of *m* are $\mathrm{diag}(m) = \left[\lambda + 2\mu\sin^2\phi, \lambda + 2\mu\cos^2\phi, \lambda\right]|u|$.

Following Day and McLaughlin (1988) we scale the doubly-integrated spall time-function by the factor v_p^2/h, where v_p is the compressional-wave velocity and *h* is the depth of the shot hole. Finally, these time functions (f_v and f_h suitably scaled) are convolved with the moment tensor for the horizontal crack and the vertical crack, respectively. The displacement at the receiver is then represented by:

$$u_n(t) = \frac{v_p^2}{h}\iint_t f_v(t)\,dt * \begin{bmatrix}\lambda & 0 & 0\\ 0 & \lambda & 0\\ 0 & 0 & (\lambda+2\mu)\end{bmatrix} G_{np,q} + \frac{v_p^2}{h}\iint_t f_h(t)\,dt * \begin{bmatrix}(\lambda+2\mu\sin^2\phi) & 2\mu\sin\phi\cos\phi & 0\\ 2\mu\sin\phi\cos\phi & (\lambda+2\mu\cos^2\phi) & 0\\ 0 & 0 & \lambda\end{bmatrix} G_{np,q} + f_{MM}(t) * \left[\delta_{pq} G_{np,q}\right] \qquad (6)$$

where u_n is the displacement vector at the receiver and $G_{np,q}$ are the Green's functions in the n direction associated with the moment tensor, m_{pq}. The moment tensor for the explosion is simply $f_{MM}\ \delta_{pq}$, the identity matrix appropriately scaled. Convolution is represented by the * symbol.

Modeling Results

In Figures 6 and 7, we have plotted the vertical velocitygrams from the vertical and horizontal spall and the explosion (for a = 240˚ and Δ = 360 km). Figure 6 is for solely vertical spall with no casting into a pit, and Figure 7 is for casting into a h_{ff} = 20 m deep pit for ϕ = 0. These signals include the time functions for the individual source contributions shown in Figure 5.

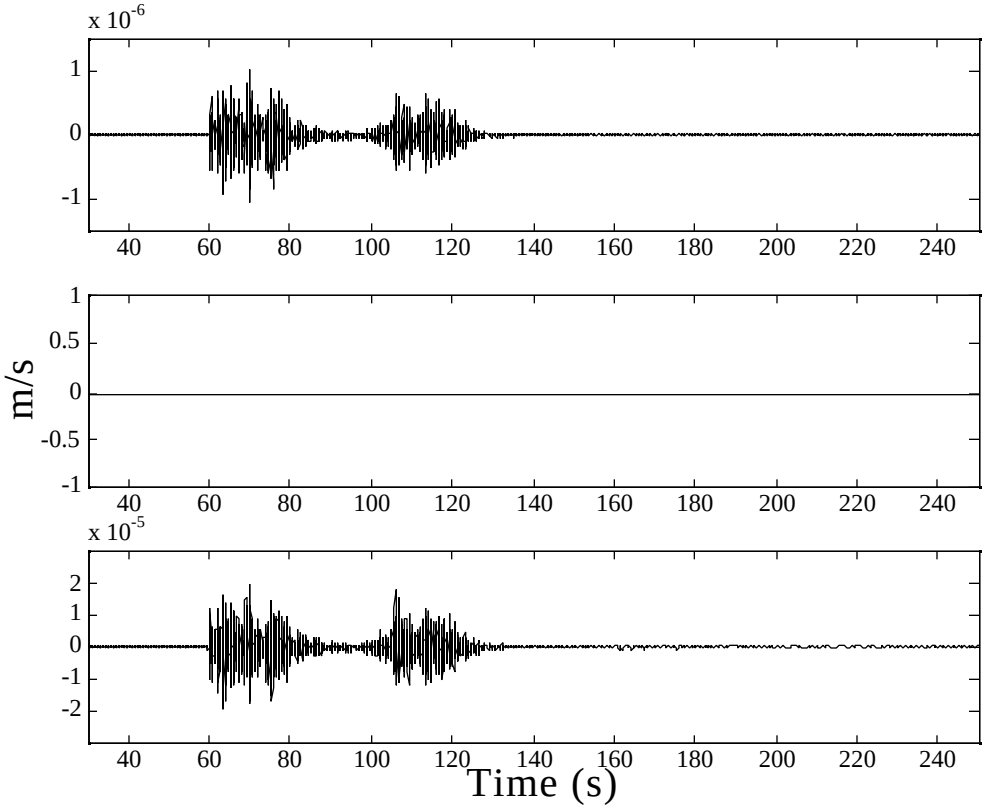

Figure 6. The three elements on the RHS of Equation 6 are shown for an explosion and vertical spall with no casting: (top) vertical spall; (center) horizontal spall (null); (bottom) explosion.

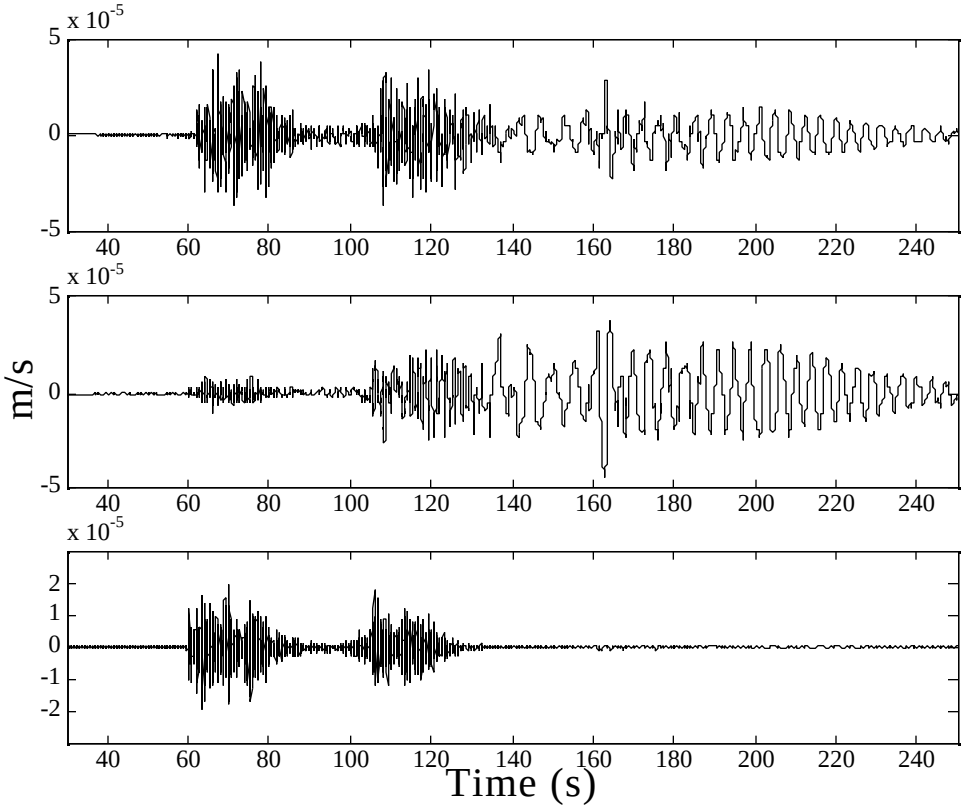

Figure 7. The three elements on the RHS of Equation 6 are shown for casting into a 20 m deep pit: (top) vertical spall including the final slapdown with the extra pit-contribution; (center) horizontal spall; (bottom) explosion.

All three elements show strong P_g (60s) and L_g (100 s) phases, with the P_n (52 s) most prominent on the explosion element. Note that P_n is very difficult to discern in many of the figures because of the velocity model used in the synthesis. In the case of no casting (Figure 6), the peak amplitude on the explosion element is approximately a factor of twenty greater than the peak on the vertical-spall contribution (there is no horizontal-spall contribution). However, in the case of casting into a 20 m deep pit, the explosion contribution is a factor of 2 smaller than either of the spall contributions (Figure 7). The P_g from the vertical spall contribution is particularly enhanced due to the force of the spalled mass falling into the pit (f_{v2} dominating) and there is enhanced low-frequency content on the spall elements that is not present in the case of no-casting. This is due to the form of

the force time-functions f_v and f_h that have two pulses separated by T_s = 2 s thus introducing a strong peak at low frequency (e.g. Taylor and Randall, 1989). This peak is not found in the explosion spectrum. Note also that on the horizontal-spall element, P_g is relatively weak (there is no extra contribution due to mass falling into the pit as there was with f_{v2}), but R_g (160 s) is strong because of the horizontal orientation of the source force. This contribution to the synthetics will depend on the azimuth of the receiver relative to the pit orientation. Bonner *et al.,* (1996), have reported on near-source (~10 km) R_g observations from small quarry blasts that exhibit a marked azimuthal variation.

As discussed above, a number of uncertainties exist in these calculations. Most notable are the estimates of the spalled mass and the coupling of the spalled energy into seismic waves. In this case, we are assuming full coupling of the secondary sources into the wavefield. Complicated nonlinear effects may alter this coupling and the relative amplitudes of the different components.

In future work we will attempt to better quantify the spall contribution through the analysis of data collected within the mine, including near-source accelerations and velocities, video of the explosions and three dimensional data from the mine. Aerial photography is conducted before and after each shot so that the total volume of material moved can be calculated. Figure 8 is an example of one of these data sets where the pit before the explosion is in gray and the pit after the explosion is in dark gray. These data can be used to quantify the mass movement estimates for the equivalent seismic source models. Attempts to relate these mass movement estimates to the total explosive usage may provide scaling relations for these secondary effects using this ground truth information.

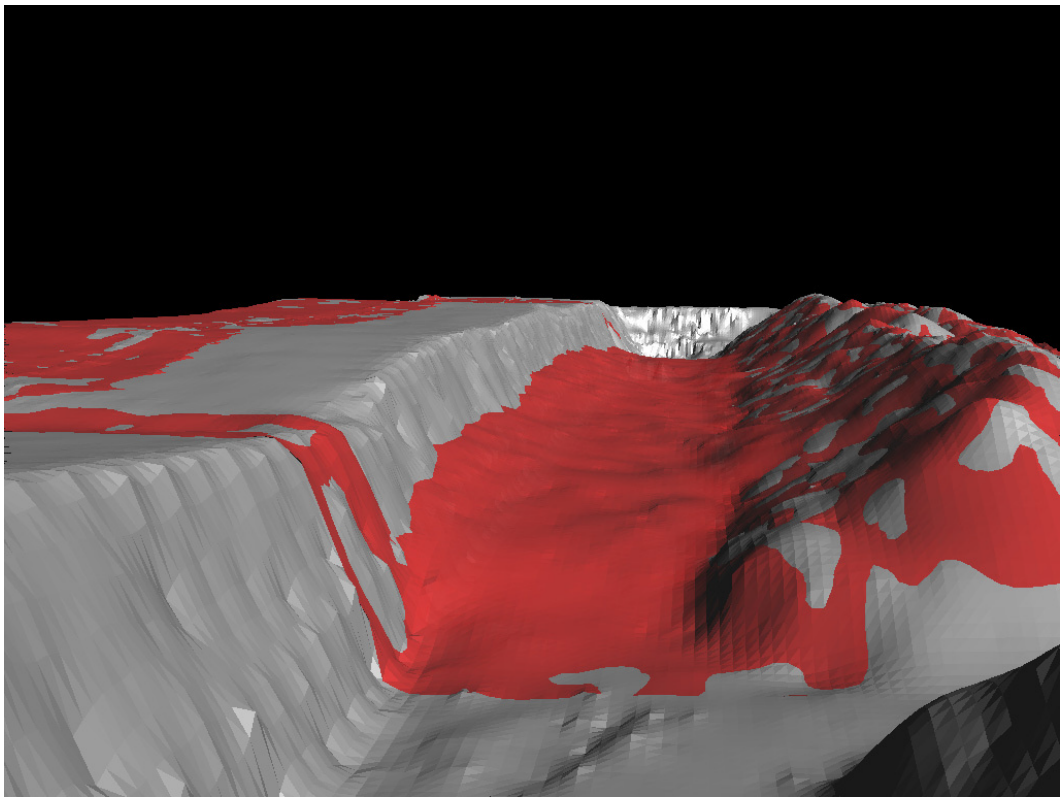

Figure 8. Three dimensional model of the mine pit before (gray) and after (dark gray) a cast blast. Data set is developed from overhead photography (see Stump *et al.*, 1996 for details).

A representative seismogram u_z is shown in Figure 9 obtained by summing the three contributions shown in Figure 7. This synthetic represents a W = 0.0025 kt source in a h = 40 m deep hole that casts material into a pit with h_{ff} = 20 m. The free-face of the pit is oriented at azimuth ϕ = 0. The casting ejection angle relative to the horizontal is θ = 10˚.

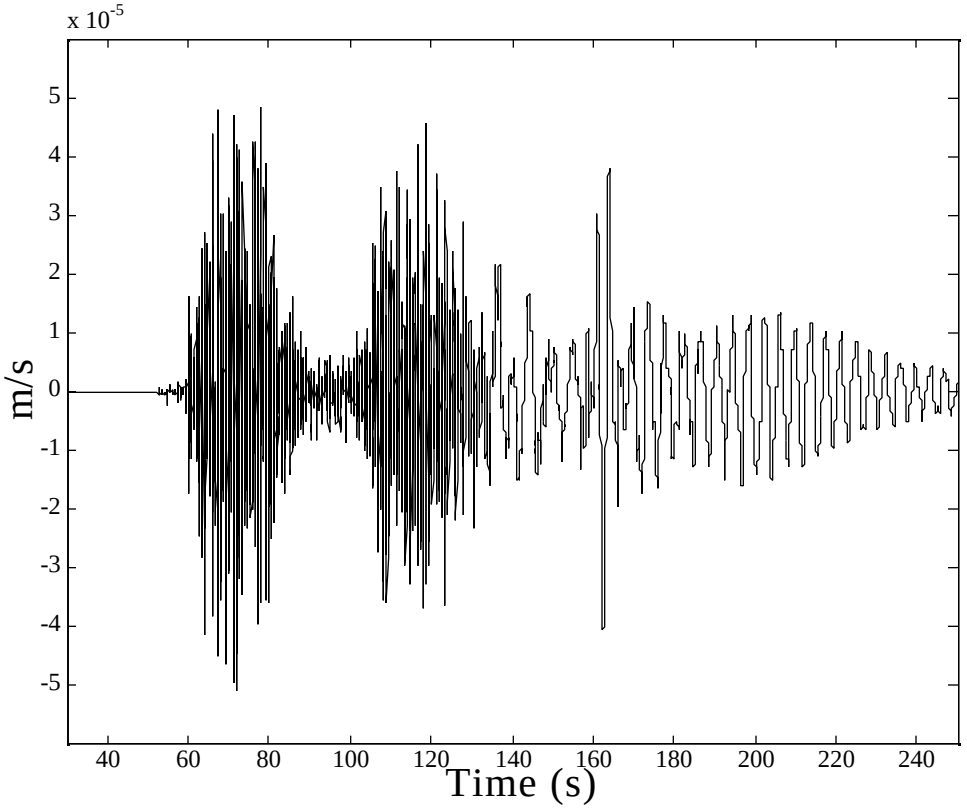

Figure 9. Final waveform resulting from adding together the contributions from the vertical and horizontal spall as well as the single explosion shown in Figure 7.

To completely represent a cast blast we next convolve the seismogram from a single hole with the millisecond delay-fire time-series (Stump and Reinke, 1988). In essence, we delay and sum one seismogram:

$$u(t) = \sum_{N} u_z\left(t - T_n - \tau_n\right) \tag{7}$$

where T_n is the shooter-imposed delay between the n^{th} and the reference (1^{st}) shot. The delay due to the geometry of the array, whereby travel time from different parts of the array to the receiver vary, is represented by $\tau_n = r_n \cos\varsigma / v_{p0}$ where r_n is the distance from n^{th} to the reference shot, ς is the angle between two vectors from the reference shot that point towards the receiver and to the n^{th} hole, respectively (Figure 10), and v_{p0} is the compressional-wave velocity in the near-surface.

We plot these time delays for the BT shot of 15 Dec 1994 at 2004 hrs (Stump *et al.*, 1996) along with the spectrum of that time series in Figure 11.

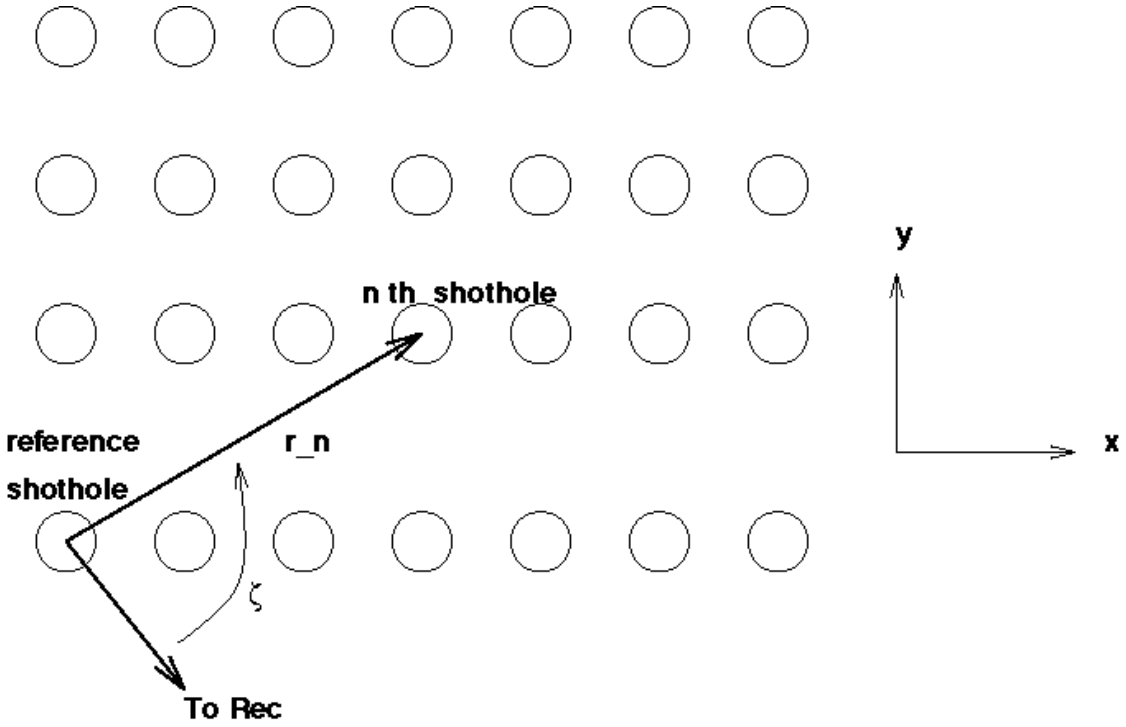

Figure 10. Map view of the shot array showing the reference shot hole and the direction vectors to the receiver and to the n^{th} hole and the angle *i* between them.

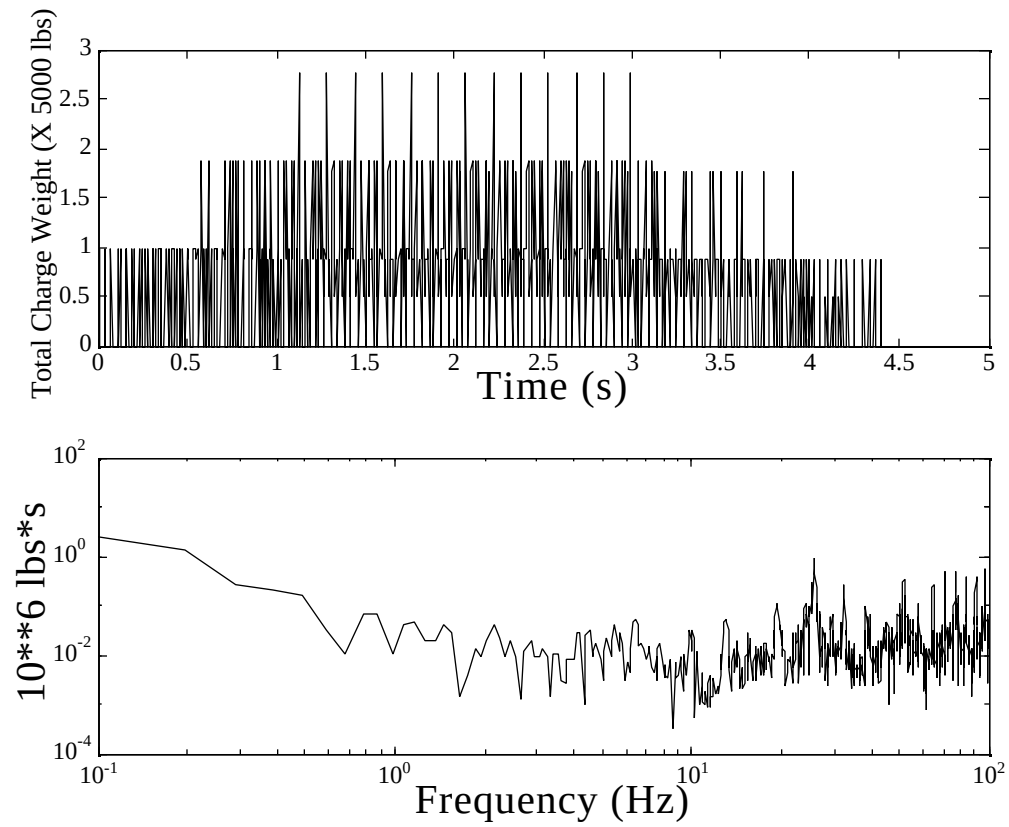

Figure 11. Time series (top) displaying the size and time of individual shots within the millisecond delay-fired cast blast shot of 15 Dec 1994 at BT. The ordinate is scaled to 5000 lb. and the abscissa is time in seconds. The bottom figure is the spectrum of the time series.

Finally, we apply a high-pass filter with a corner of 1 Hz to simulate the instrument response of an S-13 seismometer. All subsequent seismograms have had this filter applied unless stated otherwise. The resulting synthetic seismogram $u(t)$ is shown in Figure 12. The spectrum of the millisecond delay blast simulation indicates the strong low-pass filtering effect due to the finite (4 s) length of the blasting. Thus, our seismogram (which has a low-frequency corner of 1 Hz) is strongly attenuated relative to the lower frequencies that would be observed by broadband instruments.

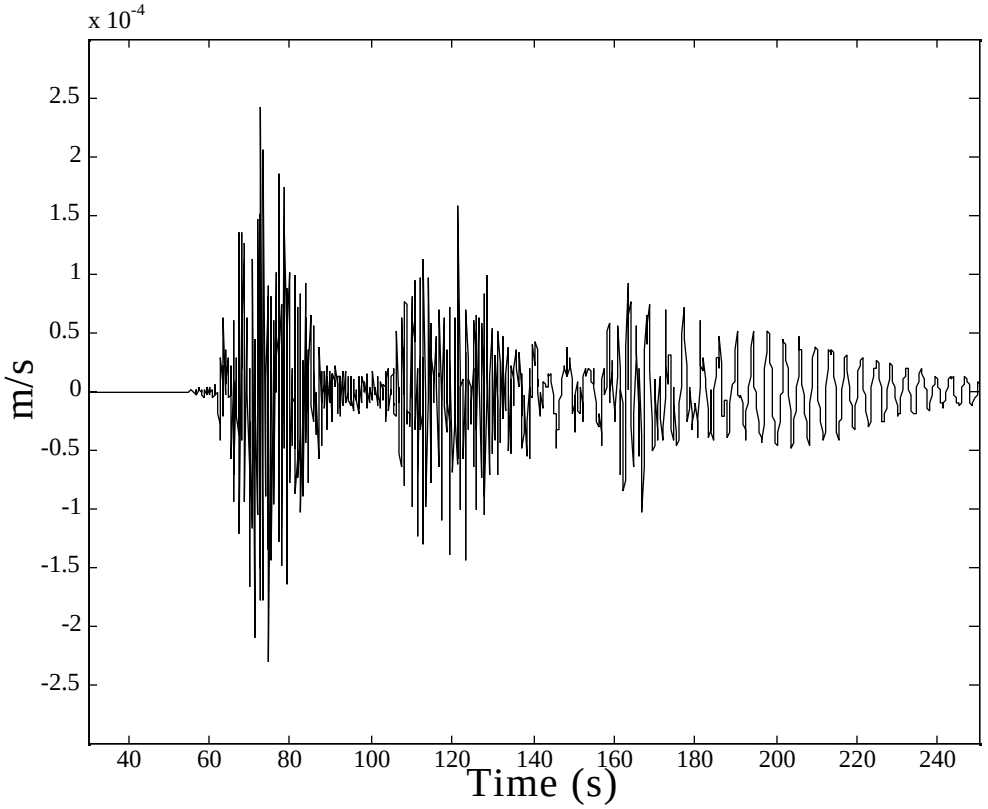

Figure 12. Final vertical component synthetic seismogram after applying the millisecond delay-fire cast blast array of the BT mine on 15 Dec 1994 to the seismogram shown in Figure 9 and applying a 1 Hz high-pass filter.

Comparisons with Black Thunder Data Recorded at PDAR

A set of experimental studies were conducted in the Powder River Basin of Wyoming in order to study regional seismic signals from large cast blasts (Stump *et al.*, 1996). Quantification of the blast characteristics included the time, location, explosive configuration and material displaced among other measures. In addition to the standard cast blasts designed to remove overburden, two additional types of explosions were documented. The second type was explosions detonated in the coal designed to fragment the material for recovery but included no casting. The third type of explosion was the simultaneous detonation of ten boreholes that were drilled and loaded away from the free

face of the mine. These boreholes were drilled to 49 m and each filled with approximately 5,000 lb of an ANFO/emulsion mixture and then backfilled to the surface. The amount of explosives and hole depth were chosen to assure that the shots would not vent to the atmosphere. In hole instrumentation at shot time indicated that only 8 of the holes fully detonated, thus suggesting the total yield was 40,000 lb.

Observed seismograms at the regional array PDAR from one of the cast blasts and the simultaneous shot are reproduced in Figures 13a and 13b respectively. The cast blast that generated these seismograms consisted of 274 holes with a total explosive weight of 2,266,178 lb. In each of these plots the vertical waveforms are displayed from the high frequency array element PD03 and the broadband seismometer PD31. The high frequency data is filtered into the bands > 1 Hz (Short Period), 2-4 Hz, 0.5-1.0 Hz and 0.125-0.250 Hz while the broadband data is filtered between 0.05-0.10 Hz without correction for instrument response. The complete waveforms and those filtered in the 2-4 Hz band from both the cast and single shot display similar characteristics although the P_g/L_g is slightly greater for the single shot. This observation is consistent with reported successes in high frequency P_g/L_g discriminants (Hartse *et al*, 1996). In the lower frequency bands, differences between the two source types are noted that are consistent with the synthetics developed in this paper.

Although this event does not have exactly the same shot-hole pattern as that used for the synthetics, it does have a similar blasting phenomenology including the large number of boreholes, casting, and material displacement. Comparison of synthetics with the observations are only included to illustrate the similar characteristics between the two including relative excitation of phases, general frequency content, and qualitative character of the seismograms.

In order to make first order comparisons with the observations, we plot the synthetic seismograms for the "cast" shot (Figure 14a) and the "simultaneous" explosion (Figure 14b) filtered in the same pass bands as the observations. Note that the large R_g phase in the calculations at 160 s is an artifact due to the trapping of energy in the undisturbed low-velocity surface layers. The lowest frequency bands, 0.125-0.250 Hz and 0.05-0.10 Hz, indicate that the cast blasts are generating significant long period energy unlike the simultaneous contained explosion. The long-period excitation observed from the cast blast, as indicated in the discussion of the synthetics below, can be attributed to either the long duration of these cast blasts or the additional source excitation resulting from the horizontal and vertical forces that represent the material cast into the pit (Equation 6). Based upon the analysis of the synthetic seismograms, the source time function including the time effects of the material cast into the pit are the likely cause of this enrichment in long period energy for cast blasts.

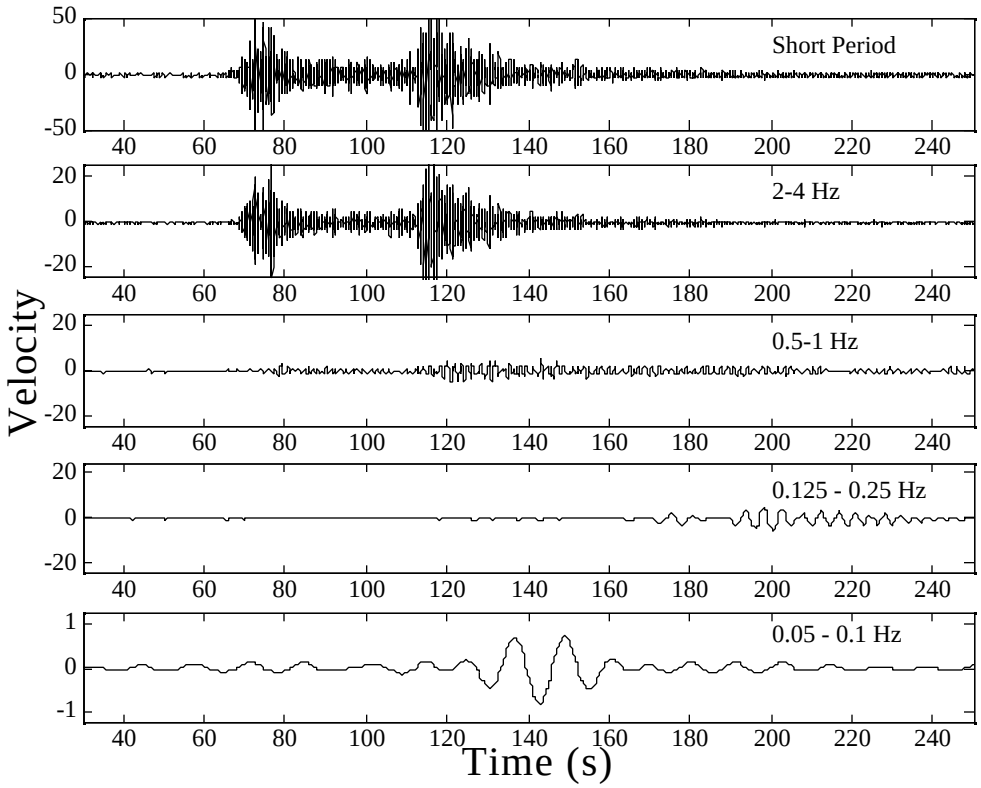

Figure 13a. Observed seismograms at the regional array PDAR from one of the Black Thunder cast blasts. The vertical waveforms displayed are from the high frequency array element PD03 and the broadband seismometer PD31. The high frequency data is filtered into the bands > 1 Hz (Short Period), 2-4 Hz, 0.5-1.0 Hz and 0.125-0.250 Hz while the broadband data is filtered between 0.05-0.10 Hz.

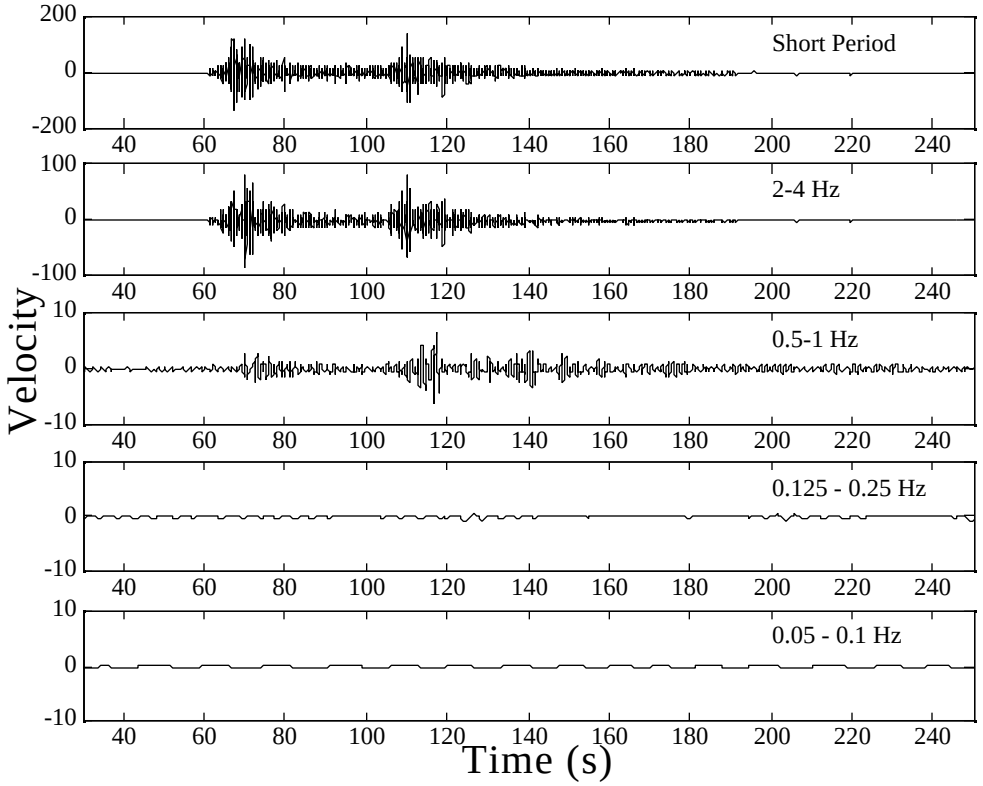

Figure 13b. Same as Figure 13a for the Black Thunder simultaneous explosion.

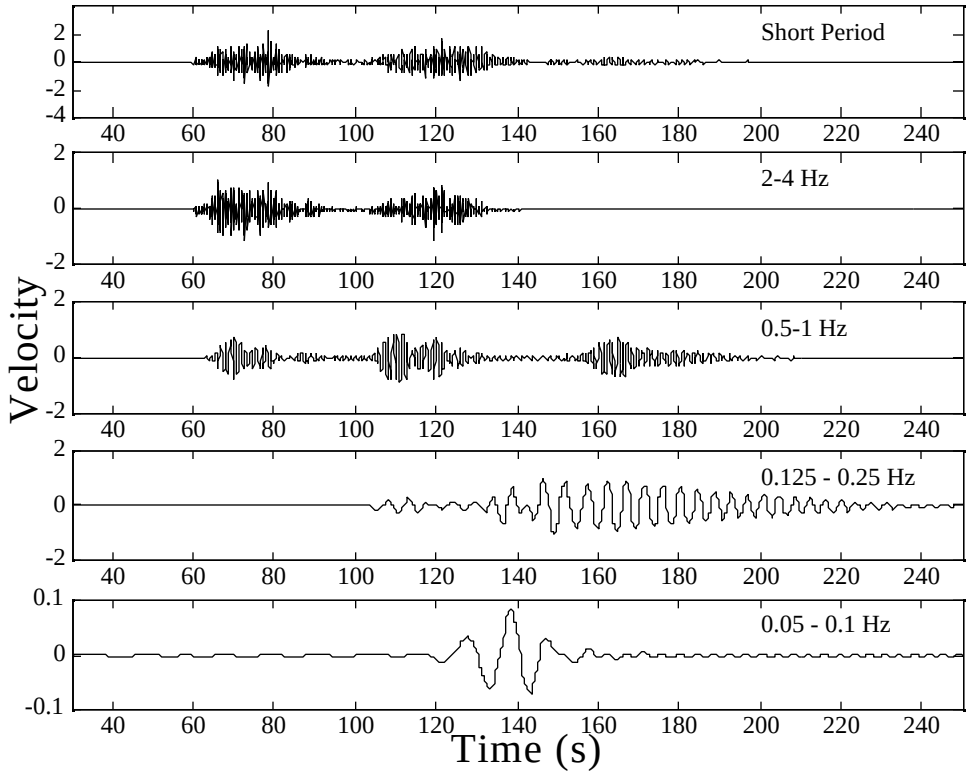

Figure 14a. Simulation of Black Thunder cast blast recorded at PDAR (Figure 13a) filtered in same pass bands as Figure 13a.

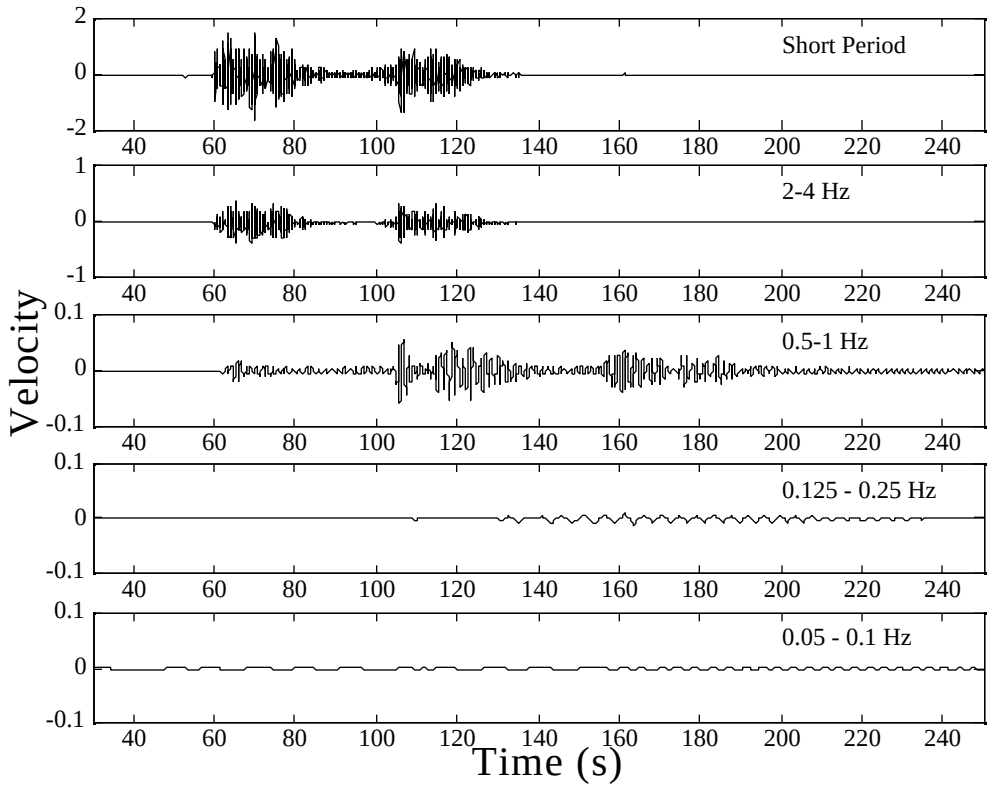

Figure 14b. Simulation of Black Thunder simultaneous explosion recorded at PDAR (Figure 6c) filtered in same pass bands as Figure 13b.

Parametric Studies

The above discussion illustrates that the simulations produce waveforms that have characteristics that are approximately similar to observations from BT at PDAR. In this section, we perform simple parametric studies to examine the effect of different parameters such as the height of the free face and the time function of the mass movement on the regional seismograms.

The main parameters that can affect the final waveform are:

1. Station azimuth *a* (degrees), distance *D* (km), and instrument response of receiver.
2. Yield W (kt) and depth *d* (m) of individual explosions.
3. Number *N* and timing of individual shots that make up the cast blast.

4. Height of free face h_{ff} (m).

5. Pulse width T_{sf} (s) of cast material impact.

6. Azimuth ϕ (degrees) of casting direction.

The values of the relevant parameters are given in Table 1 and it should be noted that we have not investigated the effects of imperfect casting in this paper. For example, the implicit assumption is that each individual shot casts its entire spall material into the pit. In reality, it is likely that only the shots in the two or three rows closest to the free face completely cast their spalled material into the pit. In addition, higher order effects such as three-dimensional and non-linear source effects are ignored. Abnormal performance of the explosions as mentioned earlier is another factor that must be taken into account. We have experimental evidence for the accidental simultaneous detonation of as much as 500,000 lb. of explosives in the midst of a standard cast blast.

TABLE 1

Parameters for Synthetics

Parameter	Value	Comments
Location-BT	43.65 N 105.25 W	Black Thunder Coal Mine
Location-PDAR	42.778 N 109.556 W	Pinedale Seismic Research Facility
Rec Azimuth	a = 240˚	
Rec Distance	D = 360 km	
Yield	W = .0025 kt	5000 lb. per hole
Number of shots	N = 700	700 individual shots made up the BT cast blast of 15 Dec 1994.
Timing	35 ms between holes in a row	Laid out in 78 "columns" of 9 holes perpendicular to the 4 km long free face
	125, 300, 500, 700,900,1000, 1200, 1400 ms between rows	
Hole depth	d = 40m	
Free face height	0,10,20m	
Impact pulse width, T_{sf}	0.1,0.5,1.0,2.0s	

Effect of Cast Blast Size

To investigate the relationship between the source yield and the observed amplitude of the signal (and thus the inferred magnitude of the source), full and subshot-array synthetics are generated and compared. Figure 15 is a plot of the three seismograms resulting from the full-, half-, and quarter-shot-array, respectively. It is apparent that the peak amplitude does not scale linearly with the source yield due to destructive interference between shots of the millisecond delay-fire pattern. Peak amplitude measurements at PDAR (short period) show little if any increase in amplitude with yield for normal Black Thunder cast blasts over the yield range of 2 to 5 million lb. At the longer periods (< 1 Hz), the peak amplitudes may scale with the total yield of the explosive array

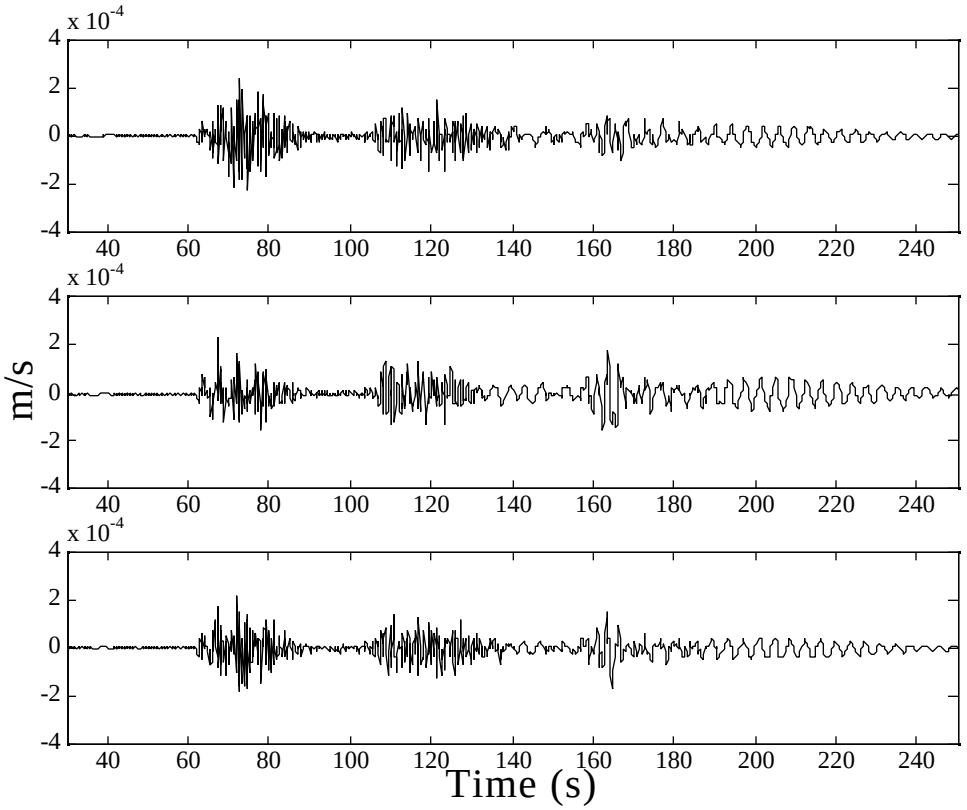

Figure 15. Vertical component synthetic seismograms resulting from firing the full (top), one-half (middle) and one-quarter (bottom) array is plotted. Thus, the yield is successively halved, but note that the peak amplitude of the resulting synthetic does not scale linearly.

Effect of Free Face Height

To investigate the contribution of the casting of material into a pit, the free-face height is variously set to h_{ff} = 0, 10, and 20 m. Figure 16 is a plot of the resulting seismograms. The peak amplitudes of P_g and L_g increase linearly with increasing h_{ff} due to the enhanced contribution of f_{v2} , the casting of mass into the pit. The seismograms for h_{ff} = 10 and 20 m show a strong R_g phase that is due to the horizontal casting based upon the comparison of horizontal and vertical spall contributions in the single source calculations (Figure 7).

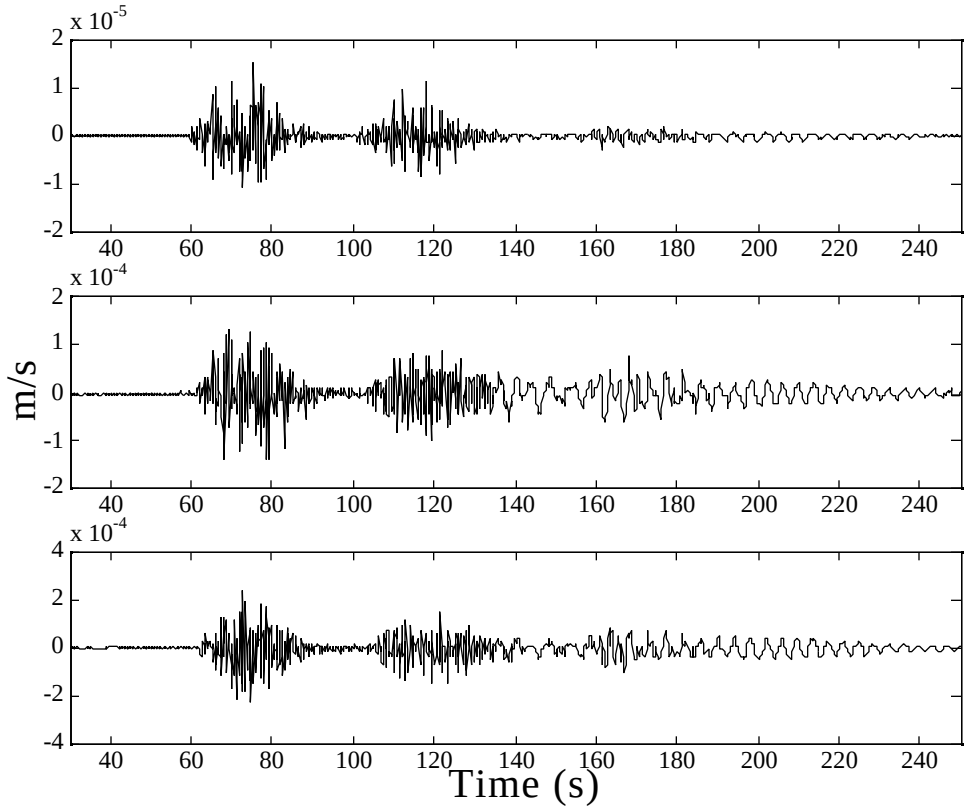

Figure 16. Vertical component synthetic seismograms resulting from free-face height set to 0 m (top), 10 m (middle) and 20 m (bottom). Note difference in amplitude scales

Effect of Time Function

We vary the impact pulse width T_{sf} = 0.108, 0.5, 1.0, and 2.0 s and plot the resulting seismograms (for a fixed free-face height of h_{ff} = 20m) in Figure 17. In general, P_g grows both larger and "spikier" with increasing T_{sf} ; note, however, that for T_{sf} = 0.5 s, P_g is a

minimum. The amplitudes of the different phases in the seismograms change in a complex way with changing T_{sf} that is apparently due to the shifting of energy into different frequency bands as T_{sf} changes.

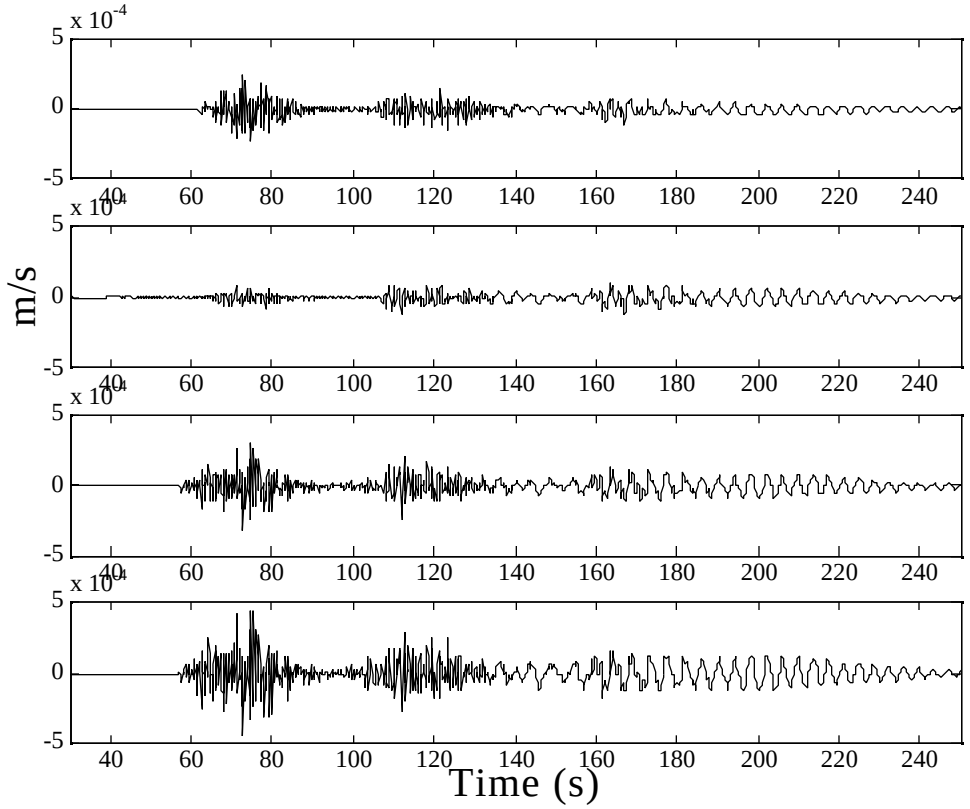

Figure 17. Vertical component synthetic seismograms resulting from impact pulse-width set to (top to bottom) 0.108, 0.5s, 1.0s, and 2.0s.

A number of different physical phenomena have been introduced into the equivalent elastic model of cast blasting (not including the complex nonlinear interactions around the explosion) including the directly coupled explosive energy, vertical spall (with and without the pit) and horizontal spall. Each source component adds its own complexity to the resulting seismograms in both the near-source region and at regional distances (e.g. Reamer *et al.,* 1992b). To illustrate two and possibly three dimensional nature of the source we modeled the spatial and temporal effects of the directly coupled compressional

energy from the over 700 individual sources. The *P* wave from each explosion was represented as a ring growing in radius with time at the *P* velocity of the in situ material. As the explosions detonate in the blast sequence, the superposition of these rings from the many individual detonations forms a two-dimensional representation of the radiated seismic energy. Four images of this process are shown in Figure 18. As time increases in the latter images, the spatial extent of each figure expands in order to capture the complete expanding wavefield.

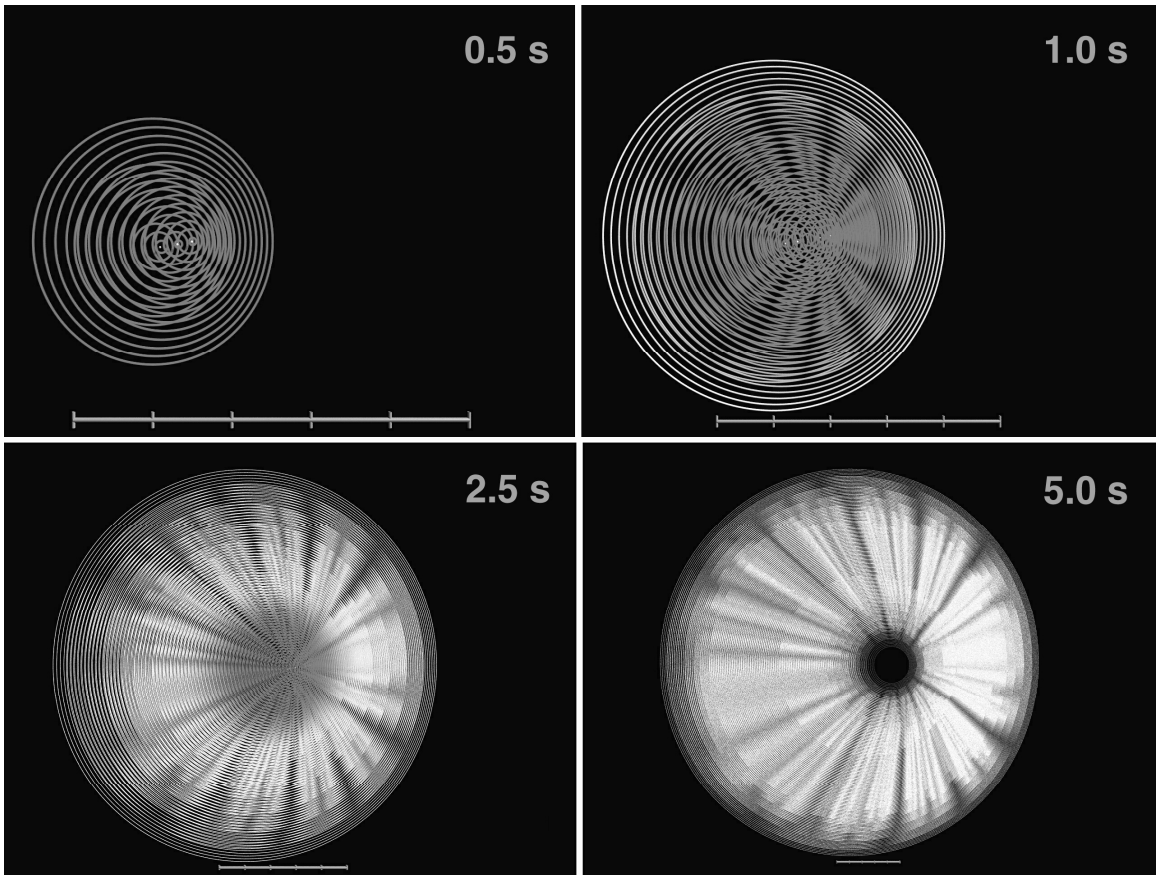

Figure 18. The constructive and destructive interference of *P* waves generated by a cast shot at four different time points (upper right hand corner). Each of the over seven hundred boreholes in the explosive array generates a *P* wave at its detonation time and spatial location that is represented by a ring expanding at the velocity of 3000 ft/s. The bar at the bottom of each image is 5000 feet long and indicates that each successive image in the sequence includes a greater area, capturing all the P wave energy.

Focusing of the *P* energy in the direction of blast propagation is illustrated as well as additional complex constructive and destructive interference patterns as a function of azimuth. Thus, both the body and surface wave energy will exhibit strong azimuthal variations. A portion of the azimuthal variation results from the focusing effects of the spatial propagation of the individual explosion (Reamer *et al.,* 1992a). Additional azimuthal variation is produced by the secondary source function representing the material cast into the pit. Quantification of the these effects at regional distances remains an open question but the observations of Bonner *et al.,* (1996), suggest that it is worth exploration.

In future work we will study discrimination techniques using both the synthetics from our model, and recorded data. The generation of very long period waves from the cast blasts, as documented in the data and replicated in the synthetics, suggests the possibility of a new discriminant for long duration cast blasts. Further quantification of the azimuthal radiation of this energy will help in the assessment of the efficacy of this proposed discriminant.

Two promising discrimination techniques are the signal subspace method and adaptive filtering that recognize signal differences such as illustrated with the cast and single shot comparison (Figure 13). A region with active coal mines might be characterized fully for the typical and normal seismic activity using signal subspace methods (Harris, 1989). Then a new signal such as the single shot could be checked against this subspace and anomalous events detected. In theory this technique is capable of extracting a single large charge detonated simultaneously with the cast-blast. A second possibility is to use traditional adaptive filtering techniques (e.g., Widrow-Hoff filtering) to detect variations from past signal character.

We also plan to study the effects of imperfect casting (i.e. modifying f_h) and to study the effects of different spall masses (e.g. using a different mass-yield estimate or estimating the mass from video of actual shots). A different explosion source function

than the one used (Mueller-Murphy) could affect the seismograms. For explosions detonated in media with high gas-filled porosity, the rate of high-frequency spectral decay appears to increase (e.g. Taylor and Denny, 1991; Jones and Taylor, 1996). The spectral content of the different phases as a function of our parameters also needs to be studied.

Conclusions

Models of cast blasting that simulate regional seismograms have been developed and compared to observational data. Model parameters for these explosions are constrained by ground truth information from the cast blasting process. The quantification of these models provides a tool for interpreting various discriminants for these event types. Validated models provide a mechanism for investigating effects of other blasting practices including anomalous or accidental detonations that sometimes accompany standard blasting operations.

The models developed in this paper are quite complex in terms of the range of effects that can be seen in the regional synthetic seismograms. Constraint of the different source contributions will require a combination of good azimuthal and frequency coverage of the regional wavefield, constraint on the regional wave propagation effects as well as quantification of the blasting practices in the mine including documentation of blast timing, spatial extent, and mass motion effects. The approach here has been to develop an equivalent elastic representation of the important physical phenomenon accompanying the explosion in order to investigate their effects on the regional seismograms. Specific consideration of nonlinear effects in the blasting process are not considered because of the difficulty in uniquely resolving their contributions to the regional seismograms with existing data.

In our model of cast blasting we have included the effects due to mass-transfer into a pit after the blast. This mass transfer has both a vertical and horizontal component, each of

which contribute to the final seismogram, the latter azimuthally dependent. The contribution to the seismogram due to the vertical component is approximately equal to the explosion-contribution for pit depths of zero to 10 m, but dominates for pit depths of 20 m or greater. The contribution due to the horizontal component is mainly in the enhanced R_g.

Long period excitation from a combination of the long source duration and casting process is found in the observational data as well as in the synthetics suggesting that these types of events might appear as earthquakes on a m_b/M_S discrimination plot. Comparison of high frequency seismic radiation from the single shot and cast blast shows little difference in the regional waveforms.

The cast blasts, in both the observations and the models, show little increase in peak regional amplitude with yield, a reflection of the delay firing practice under normal procedures. This practice was initiated to reduce ground motions in the near-source region around the mine and it appears that it is also successful in controlling peak amplitudes at regional distances.

Acknowledgments

We would like to thank D. Craig Pearson for reviewing the manuscript and aiding in the collection of all of the good data, Vindell Hsu (AFTAC) for providing regional data from PDAR, and David Anderson for help with imaging some of the two and three dimensional data sets. The experimental data could not have been gathered and this project could not have been completed without the close cooperation and advice from Robert Martin and David Gross of the Thunder Basin Coal Company, Black Thunder Mine, ARCO. This work is performed under the auspices of the U.S. Department of Energy by Los Alamos National Laboratory under contract W-7405-ENG-36.

References

Aki, K. and P. G. Richards. Quantitative Seismology. Theory and Methods. W.H. Freeman and Co., 1980.

Bonner, J. L., E. T. Herrin and T. T. Goforth, Azimuthal variation of R_g energy from quarry blasts in central Texas, *Seism. Res. Letters*, **67**, 43-56, 1996.

Day, S. M., N. Rimer, and J. T. Cherry. Surface waves from underground explosions with spall: analysis of elastic and nonlinear source models. *Bull. Seism. Soc. Am.*, 73, 247-264, 1983.

Day, S. M., and K.L. McLaughlin, Seismic source representations for spall, *Bull. Seism. Soc. Am.*, 81, 191-201, 1991.

Harris, D. B. and G. A. Clark, Effects of delay shooting on the nature of P-wave seismograms, *Bull. Seis. Soc. Am.*, 70, 2037-2050, 1990.

Harris, D. B., Characterizing source regions with signal subspace methods: Theory and computational methods, Lawrence Livermore National Laboratory, UCID-21848, 41 pp, 1989.

Hartse, H.E., S.R. Taylor, W.S. Phillips, and G.E. Randall, Regional event discrimination in central Asia with emphasis on western China, *Los Alamos National Laboratory, Los Alamos, NM*, LAUR-96-2002, 45pp, submitted to *Bull. Seism. Soc. Am.*, 1996.

Hedlin, M. A. H., J. B. Minster, and J. A. Orcutt, The time-frequency characteristics of quarry blasts and calibrations explosions recorded in Kazakhstan, USSR, *Geophys. J. Int.*, 99, 109-121, 1989.

Hedlin, M. A. H., J. B. Minster, and J. A. Orcutt, An automatic means to discriminate between earthquakes and quarry blasts, *Bull. Seis. Soc. Am.*, 80B, 2143-2160, 1990.

Jones, E.J., and S.R. Taylor, Are Lg spectra from NTS self similar? *Bull. Seism. Soc. Am.*, 86, 445-456, *Bull. Seism. Soc. Am.*, 86, 445-456, 1996.

Kennett, B. L. N, Seismic Wave Propagation in Stratified Media, Cambridge University Press, Cambridge, 342 pp., 1985.

McLaughlin, K.L., T.G. Barker, J.L. Stevens, and S.M. Day, Numerical simulation of quarry blast sources, in Proceedings of the 15th Annual PL/DARPA Seismic Research Symposium, edited by J.F. Lewkowicz and J.M. McPhetres, PL-TR-93-2160, 263-268, 1993.

Mueller, R. A. and J. R. Murphy, Seismic characteristics of underground nuclear detonations, Part 1; seismic spectrum scaling, *Bull. Seis. Soc. Am.*, 61, 1675-1692, 1975.

Patton, H.J., Characterization of spall from observed strong ground motions on Pahute Mesa, *Bull. Seism. Soc. Am.,* 80, 1326-1345, 1990.

Prodehl, C, Crustal structure of the western United States, U.S. Geol. Surv. Prof. Paper 1034, 1979.

Reamer, S.K., and B.W. Stump, Source parameter estimation for large, bermed, surface chemical explosions, *Bull. Seism. Soc. Am.,* 82, 406-421, 1992a.

Reamer, S. K., K.-G. Hinzen and B. W. Stump, Analysis of spatial and temporal finiteness observed in the seismic wavefield radiated from quarry blasts, *Geophys. J. Int.,* 110, 435-450, 1992b.

Sobel, P.A., The effect of spall on m_b and M_s, Teledyne Geotech Rept. SDAC-TR-77-12, Dallas, Texas, 1978.

Smith, A. T., High-frequency seismic observations and models of chemical explosions: Implications for the discrimination of ripple-fired blasts, *Bull. Seis. Soc. Am.,* 79, 1089-1110, 1989.

Smith, A. T., Discrimination of explosions from simultaneous mining blasts, *Bull. Seis. Soc. Am.,* 83, 160-179, 1993.

Stump, B. W. and R. E. Reinke, Experimental confirmation of superposition from small-scale explosions, *Bull. Seis. Soc. Am.,* 78, 1059-1073, 1988.

Stump, B. W., D. C. Pearson, C.L. Edwards, and D. Baker, Experimental studies for event identification, system calibration and evasion assessment: A progress report, Los Alamos National Laboratory, LAUR-96-1187, 42pp, 1996.

Stump, B. W, Constraints on explosive sources with spall from near-source waveforms. *Bull. Seis. Soc. Am.,* 75, 361-377, 1985.

Taylor, S.R. and G.E. Randall, The effects of spall on regional seismograms, *Geophys. Res. Lett.,* 16, 211-214, 1989.

Taylor, S.R., and M.D. Denny, An analysis of spectral differences between NTS and Shagan River nuclear explosions, *J. Geophys. Res.,* 96, 6237-6245, 1991.

Viecelli, J.A., Spallation and the generation of surface waves by an underground explosion, *J. Geophys. Res.,* 78, 2475-2487, 1973.